Algorithm Theoretical Basis Document: Algorithms to Validate NISAR L2 Coseismic, Transient and Secular Displacement Requirements

Revision A

May 25, 2022

NISAR Solid Earth Team

The NISAR Algorithm Theoretical Basis Documents (ATBDs) provide the physical and mathematical descriptions of algorithms used in the generation of NISAR cal/val science data products. The ATBDs include descriptions of variance and uncertainty estimates and considerations of calibration and validation, exception control and diagnostics. Internal and external data flows are also described.

The NISAR ATBDs were reviewed by a NASA Headquarters review panel in summer 2022, with initial public release on [TBD]. The current version is Revision A. The ATBDs may undergo additional version updates after NISAR launch.

1. INTRODUCTION

This Algorithm Theoretical Basis Document (ATBD) describes the algorithms used by the NISAR project to validate Solid Earth Science (SES) Level 2 (L2) requirements 658, 660 and 663 for, respectively, observing steady secular movement, co-seismic ground offsets, and transient deformation (see Section 3), where deformation of the solid earth includes surface motion in regions underlain by permafrost.

To carry out this validation requires generating and analyzing a suite of Level 3 data products from lower-level data, as described in this ATBD. The NISAR Project will produce these lower-level data products for distribution to the NISAR science team and to the entire science community, using a common set of algorithms that are described in the NASA SDS Algorithm Theoretical Basis Document (JPL D-95677, released September 18, 2019). A definition of data product levels and a description of the associated data products for the NISAR mission is available in the *NISAR NASA SDS Product Description* document and in chapter 5 of the *NASA-ISRO SAR (NISAR) Mission Science Users' Handbook* (2018).

NISAR will measure ground displacements over time through the well-established technique of repeat-pass interferometry (e.g., *Goldstein et al*., 1993; *Massonnet et al*., 1993; *Zebker et al*., 1994; *Bamler and Hartl*, 1998; *Massonnet and Feigl*, 1998; *Bürgmann et al*., 2000; *Rosen et al.,* 2000; *Hanssen*, 2001; *Simons and Rosen*, 2015), wherein radar images acquired from nearly the same vantage point over time are compared interferometrically, with the phase difference between images representing ground displacement plus unmodeled atmospheric delay and noise.

NISAR will acquire near-global coverage of the surface of the solid Earth, including tectonically active areas and other locations where non-tectonic surface deformation is occurring. NISAR will measure at least two components of the surface displacement vector field by making observations on both ascending (southeast/northwest) and descending (southwest/northeast) paths. These two independent observations along the satellite line-of-sight directions can be used to separate the horizontal and vertical components of the vector displacement field. We note that while Level 2 requirements specify validation of two components of motion, this ATBD discusses only a single component under the assumption that the same validation will be used for the other component as well. Additionally, while NISAR has left and right looking capability, the current mission plan specifies—and this ATBD assumes—left-looking observations only.

For the sake of simplicity, the SES mission requirements are framed in the context of tectonics. Since various non-tectonic motions can be described in terms of styles of tectonic deformation, the broader applicability of the SES requirements is assumed. Examples of non-tectonic NISAR applications include monitoring changes in energy and water resources, mapping degradation of permafrost in the Arctic, imaging surface deformation associated with anthropogenic activities, and remote assessment of the national transportation infrastructure, all of which will benefit from high resolution maps of surface displacements over time.

1.1. Motivation: Secular Velocities

The measurement of secular velocities plays an essential role in our understanding of fundamental processes associated with tectonic deformation and post-glacial rebound, along with many other gradual and steady processes that deform Earth's surface. Secular velocities in the context of NISAR also refer to the approximately constant velocity fields associated with other processes whose time scales exceed the operational lifetime of the mission. NISAR will be able to separate vertical and horizontal components of the secular velocity field by measuring at least two components of motion on ascending and descending paths.

Tectonic deformation*:* Measurements of secular velocities in plate boundary regions are foundational to our basic understanding of fault physics and place important constraints on models of tectonic deformation, thereby contributing to estimates of long-term seismic hazard. The average rate of strain accumulation or long-term seismic potential of a fault is directly proportional to the product of the rate at which the fault is loaded by motions of the plates (i.e., the long-term slip rate) and the area of the fault that is locked in the times between large earthquakes. The average slip rate is typically equivalent to the relative velocity across the fault measured over a 50 km length scale (Savage, 1983; Savage and Burford, 1973). The area of the fault that is locked can be estimated using the velocity gradient over shorter distances. At least two of the three components of the vector field of relative velocity are needed to distinguish the strike and the dip components of the slip vector on the fault and to infer along-strike variations in locking. NISAR will image most of the subaerial portions of Earth's plate boundary zones from two different directions, sampling the range of different tectonic styles, capturing plate boundaries at different stages of the earthquake cycle, and informing regional assessments of seismic hazard.

Post-glacial rebound*:* The earth is continuously readjusting to the historical redistribution of water and ice masses associated with the retreat of the Pleistocene ice sheets, as well as ongoing melting of remaining glaciers, ice caps, and ice sheets. This readjustment, known as "glacial-isostatic adjustment" (GIA), includes both an instantaneous elastic response to current changes in water/ice loading and an ongoing viscoelastic response associated with past changes in loading, from the present day to thousands of years ago. Understanding surface deformation from GIA has important implications for our ability to predict sea level rise (SLR) and to interpret regional-scale gravity observations from space. Improving this understanding depends upon the history of ice loading, with competing models of ice loading predicting vector velocities that differ by 2 mm/yr over 50 km length scales. Accurate SLR predictions are also tied to our understanding of the rheological (viscoelastic) structure of the mantle, with different structural models predicting different patterns of surface deformation.

Other longer time-scale processes*:* For some processes, separating secular velocities from time-variable motion is key to characterizing the physics of the underlying phenomenon. One example of this arises in measurements of displacement over aquifers, in which it is necessary to separate the inelastic subsidence that permanently reduces the storage capacity of an aquifer from the annual subsidence/inflation due to water use

patterns. Since proper management of the aquifer system depends on maintaining the long-term storage of the system, NISAR must be able to resolve these different motions. A similar situation occurs with permafrost degradation, where secular subsidence relating to permafrost decay needs to be separated from quasi-seasonal deformation caused by the freeze-thaw cycle of the overlying active layer (*Liu et al*, 2010; *Liu et al*, 2012). A separate ATBD covers observations of permafrost.

1.2. Motivation: Coseismic Displacements

NISAR will map the large deformation that occurs during or shortly after an earthquake at most Earth locations using a small number of interferograms. Measuring displacements associated with earthquakes is essential for 1) describing which segments of a fault have ruptured, 2) determining which fault segments have not ruptured but may have been brought closer to failure, and 3) constraining estimates of the distribution of fault slip in the subsurface. Estimates of other rupture characteristics, such as the speed at which rupture propagates along the fault and the rate at which slip occurs at a given point on the fault, are also best constrained by combining seismic data with coseismic displacement information such as will be provided by NISAR, as opposed to using seismic data alone (e.g., *Pritchard et al*., 2006; 2007; *Duputel et al*., 2015). These estimates of fault slip parameters then provide key input into mechanical models of faults and the surrounding crust and upper mantle, provide estimates of stress change on neighboring faults, and inform our basic understanding of regional seismic hazards.

For most earthquakes, it is important to be able to observe both vertical and horizontal displacements in order to constrain strike and dip (3D) components of fault slip. NISAR will achieve the necessary sensitivity to vertical and horizontal deformation by measuring at least two components of the relative fault displacements through ascending and descending acquisitions.

1.3. Motivation: Transient Deformation

Detecting and quantifying transient deformation is essential for improving our understanding of fundamental processes associated with tectonics, subsurface movement of magma, volcanic eruptions, landslides, the solid earth response to changing surface loads, surface motion due to thawing and freezing of permafrost, and a wide variety of anthropogenic phenomena.

Aseismic and post-seismic fault slip transients, volcanic and landslide deformation, and local subsidence and uplift due to migration of crustal fluids occur globally over a large range of temporal (sub-daily to multi-year) and spatial (10 m to 100s km) scales. NISAR is targeting nearly 2000 sites of known or possible transient deformation, including: approximately 1400 active volcanoes; post-seismic deformation from dozens of earthquakes; a representative sample of landslides, groundwater aquifers, hydrocarbon reservoirs, and geothermal reservoirs; as well as locations of rapid surface motion due to changing surface loads such as melting glaciers.

Anthropogenic and climate-sensitive measurements both require adequate sampling to resolve annual or shorter components of the displacement time history. For example, annual deformation cycles over aquifer systems often result from groundwater withdrawal and recharge. NISAR's target sites include some with human-induced deformation due to oil/gas mining and geothermal energy production, which can vary over arbitrary time scales. Observations of these transient motions are best supported by resolving deformation at the shortest time scale possible, since it is not known in advance how a particular phenomenon might evolve. In the context of NISAR, we will be able to uniquely constrain the temporal evolution of transient displacements in the line-of-sight direction at time scales of twice the repeat acquisition time in a given overflight direction (ascending or descending). The effective temporal resolution for obtaining two-component displacements will be determined by the repeat timing of both ascending and descending passes over the area of interest.

The detection and quantification of transients is perhaps the most exciting frontier of solid earth deformation science. The greatest challenge to robust detection of transient deformation is the unknown temporal and spatial behavior of many of the associated processes and the need to isolate transient signals in the presence of other processes such as impulsive events (e.g., earthquakes), quasi-periodic seasonal signals (which may not necessarily be a pure single annual sinusoid), and secular trends. Any transient phenomenon can be considered to be a specific case of the general problem of transient detection, which means that addressing the needs of the solid Earth science community largely ensures the applicability of the mission to a wider audience.

2. THEORETICAL BASIS OF ALGORITHMS

Here we describe the three Solid Earth Science (SES) validation requirements and the underlying physical (forward) model that is assumed for each. As noted above, satisfying these three specific requirements will ensure that NISAR observations can be applied to many other applications covering a broad spectrum of crustal deformation phenomena.

2.1. Requirements

The three primary NISAR Solid Earth Sciences L2 requirements that drive the L3 products needed for calibration and validation are:

L2 Requirement 658 - Secular Deformation Rates: *Over three years, the NISAR project shall measure at least two components of the spatially and temporally averaged relative vector velocities over active regions of Earth's land surface with accuracy of 2 mm/yr or better, over length scales 0.1 km < L < 50 km, over 70% of these regions.*

The NISAR mission identifies actively deforming regions of Earth using the Kreemer et al. (2014) Global Strain Rate Model (GSRM). Regions are defined as active if the GSRM indicates strain in excess of 20 ns/yr or 1 mm/yr over 50 km and are identified in the Secular Deformation Targets Map in Appendix H of the NISAR handbook (2018). To meet the requirement, NISAR must be able to constrain displacements in two look directions (left-looking on both ascending and descending tracks for current mission

configuration) for 70% of Earth's active regions with an accuracy of 2 mm/yr root-mean-square. By relative vector velocities we refer to the difference in measured velocity between any two points over the three years. This requirement refers to secular velocities measured over up to three years. In areas with high correlation, several acquisitions spanning the three years may be sufficient, while in other areas many acquisitions would be needed. This requirement applies to 70% of the area of active regions imaged by NISAR. Decorrelation or significant atmospheric artifacts may preclude the formation of high-quality interferograms in some areas.

L2 Requirement 660 - Coseismic Deformation: *Over three years, the NISAR project shall measure at least two components of the point-to-point vector co-seismic displacements of at least 80% of regions where earthquakes with sufficient magnitude to generate surface displacements of 100 mm or greater occur, with accuracy of* $4\ (1+L^{1/2})$ *mm or better, over length scales 0.1 km* $< L <$ *50 km, at 100 m spatial resolution over at least 70% of these regions.*

During the course of the three-year primary mission, NISAR must be able to constrain displacements in two look directions (left-looking on both ascending and descending tracks) for 80% of Earth's earthquakes with sufficient magnitude to cause displacement on land of 100 mm or more. The point-to-point displacement accuracy scales with baseline distance L between any two locations within a scene. Here, accuracy is calculated using L in kilometers but with the units removed, at 100 m resolution. The accuracy then is 5 – 32 mm for distances ranging from 0.1 – 50 km over at least 70% of the regions. Errors introduced by unmodeled tropospheric path delay cause the accuracy to be degraded over longer distance scales (*Donnellan et al.*, 2018).

L2 Requirement 663 – Deformation Transients: *The NISAR project shall measure at least two components of the point-to-point vector displacements over at least 70% of targeted sites with accuracy of* $3\ (1+ L^{1/2})$ *mm or better, over length scales 0.1 km* $< L <$ *50 km, at 100 m resolution, and over 12-day time scales.*

NISAR must be able to constrain displacements in two look directions (left-looking on both ascending and descending tracks) for the active area of 70% of target sites with an accuracy that scales with baseline distance L between any two locations within a scene. This pertains to all directly measured or inferred 12-day interferograms over the duration of the mission. Here, accuracy is calculated using L in kilometers but with the units removed, at or better than 100 m resolution. The 12-day time scale corresponds to a repeat NISAR pass on each of the ascending and descending satellite tracks, from which interferograms can be made and displacements estimated. The NISAR mission has compiled a list of 2000 global targets covering areas of known or potential transient deformation related to the processes specified in the requirement (NISAR Handbook Appendix H, 2018). These targets include all Earth's active volcanoes above sea-level, areas of rapid glacial mass changes, selected deforming reservoirs of water, oil, gas, CO2 and steam and landslide-prone areas near major population centers, as well as sites where selected disaster-related events have occurred.

2.2. Approaches to validating the L2 requirements

We use three approaches for validating the NISAR Solid Earth Science L2 requirements. All approaches require L2 data inputs in the form of unwrapped NISAR interferograms over calibration/validation (cal/val) targets that sample a range of vegetation types, topographic relief, and strain rates. Requirement 663 (Transients) requires individual interferograms only. Requirements 658 (Secular) and 660 (Coseismic) require a set of temporally contiguous/overlapping SAR interferograms over all time periods of interest, from which deformation timeseries can be generated (see description of inputs and potential preprocessing steps in Sections 3 and 5).

For Validation Approach #1, we compare InSAR-derived surface displacements with point observations of surface motion from collocated continuous GNSS stations (hereafter we refer to continuous GNSS simply as "GNSS"). Since all requirements are written in terms of relative displacements between individual points within the deformation field, comparisons are done using the differences of observed surface motion (from both InSAR and GNSS) between GNSS station locations. For a GNSS station network of N stations located within an interferogram, this will yield $N(N\text{-}1)/2$ distinct observations for comparison, distributed across a range of length scales. As we discuss below, the methodology differs slightly depending on whether we perform our comparison using displacements from single interferograms (Requirement 663) or using basis functions fit to deformation time series derived from many interferograms (Requirements 658, 660), but the underlying premise is the same: that GNSS provides a sufficiently high-quality time series to validate InSAR observations. This approach is appropriate where measurable displacements are occurring across the cal/val region and the GNSS network is sufficiently dense to capture most of the expected spatial variability of the signal.

For Validation Approach #2, which is appropriate for negligibly deforming regions, we examine the NISAR interferograms without comparison to GNSS, under the assumption that surface deformation is equivalently zero at all relevant spatial scales. This method involves computing InSAR displacement observations at a statistically significant number of randomly chosen interferogram pixels and confirming that the estimates are consistent with there being no deformation within the scene.

For Validation Approach #3, which can be blended with the first two approaches, we use UAVSAR to validate the InSAR-derived motions at scales smaller than the characteristic spacing between the GNSS stations. UAVSAR has the advantage of filling in the spatial sampling between GNSS stations at a resolution approximately 10X higher than the resolution of NISAR images. Ideally, UAVSAR data will be collected during NISAR passes. Corner reflectors will further validate the accuracy and can be used to assess UAVSAR motion compensation errors. Assessment of UAVSAR motion compensation errors should be carried out prior to NISAR launch from experiments using corner reflectors that are moved between passes. **Note: this ATBD does not fully specify details of the implementation of Validation Approach #3.**

All the Solid Earth Science L2 requirements specify a minimum spatial coverage component, whose validation will rely on a combination of assessing the coverage of InSAR-quality data and ensuring that the required measurement accuracy is achieved in a suite of locations that comprehensively sample different types of regions with respect to surface properties and vegetation land cover. Many of these regions will be automatically evaluated as part of the targeted sites for the transient deformation requirement.

2.2.1. L2 Requirement 658 - Secular Deformation Rate

To validate relative secular deformation rates (or velocities) from NISAR, we use Line-of-Sight (LOS) velocity data for each coherent pixel in a target region. We generate separate LOS velocities for ascending and descending passes to meet the requirement for two components of motion over each target location. Although the requirement specifies that the validation span 3 years of data, we can perform the validation for periods shorter than 3 years provided we mitigate annual effects by using data that span multiples of 1 year, or by explicitly modeling and removing the seasonal displacements. The relative vector velocity between any two points in the scene will be taken as the difference in the LOS velocity at those points.

In Validation Approach #1, we use the LOS velocity product to calculate the relative InSAR velocity between each pair of GNSS stations within the SAR footprint that are less than 50 km apart. We then generate the accompanying GNSS velocity differences by projecting the 3-component GNSS position time series into the InSAR LOS direction, estimating the GNSS LOS velocities, and differencing the GNSS LOS velocities between all station pairs. To test NISAR's fulfillment of the 2 mm/yr specification, we difference the InSAR and GNSS relative velocity estimates for each pair, and perform the statistical tests discussed in Section 4.2.1.

Validation Approach #2 is similar to approach #1 except that the relative velocities are determined for random pairs of InSAR pixels within a scene assumed to have no deformation. The statistics are calculated directly from the InSAR estimates, since it is assumed that any GNSS velocity would be zero. The cal/val regions to be used for both approaches will be defined by the NISAR Science Team and listed in the NISAR cal/val document.

For Validation Approach #3, we fly UAVSAR campaigns in ascending and descending tracks over areas identified as not deforming, preferably with corner reflectors, and areas with a clear deformation signal such as the creeping section of the San Andreas fault in California and the Slumgullion Landslide in Colorado. UAVSAR campaigns should take place over regions that have GNSS stations present throughout the swath and that are assessed to have surface motions that are not greatly affected by anthropogenic, seasonal, or ground water signals. UAVSAR and GNSS will validate assumptions for NISAR that regions are not deforming or demonstrate that they are deforming for comparison to NISAR and external validation. UAVSAR image swaths will be collected along two sets of flight paths, with the first optimized for measuring motion of the observed feature and the second in the direction of NISAR ascending and descending passes.

2.2.2. L2 Requirement 660 - Coseismic Displacements

To validate NISAR's ability to recover relative coseismic displacements of 100 mm and larger within a scene, step functions in surface displacements are estimated at the time of an earthquake from InSAR and GNSS time series.

The simplest version of the InSAR estimate is a coseismic interferogram spanning the earthquake, assuming negligible post-seismic deformation. Greater accuracy can be obtained by modeling an InSAR time series using appropriate basis functions (e.g., a secular displacement rate, a Heaviside time function at the time of the earthquake, and an exponential postseismic response) and using the offset thus obtained. Similar analysis is done for the GPS time series. To validate the requirement for two components of motion, we separately analyze ascending and descending passes over each target location.

In Validation Approach #1, relative displacements will be calculated between each pair of GNSS stations within the relevant interferograms over a timespan spanning an earthquake and less than 50 km apart. To do the comparison, coseismic displacements from GNSS are estimated by estimating the amplitude of a Heaviside basis function at the time of the earthquake for the 3-component GNSS positions. The InSAR displacements are treated the same way. The GNSS 3-component displacements are then projected onto the InSAR line of sight direction and differenced to obtain the relative GNSS displacements between all station pairs. To test NISAR's fulfillment of the $4(1+L^{1/2})$ mm accuracy requirement, the InSAR and GNSS relative displacement estimates are differenced for each pair of GNSS station locations. The baseline distance L between stations and the mean and standard deviation of all residuals are calculated, then we perform the statistical tests described in Section 4.2.1 to check whether the mean error is statistically less than $4(1+L^{1/2})$ mm over length scales 0.1 km $< L <$ 50 km (e.g., $\leq$ 5 mm at 0.1 km and $\leq$ 32 mm at 50 km).

Validation Approach #2 for Coseismic Displacements is similar to Approach #1 and Approach #2 for Secular, except we use the relative InSAR displacements instead of velocities. The relative displacements are determined for random pairs of InSAR pixels within a scene that does not include a significant deformation, and the statistics are calculated directly from the InSAR estimates of displacement from a Heaviside function fit at an arbitrary time in a time-series.

2.2.3. L2 Requirement 663 - Transient Displacements

To validate the L2 requirements on transient displacements, we will produce 12-day interferograms from both descending and ascending tracks over diverse target sites where GNSS observations are available. The two components of vector displacement, ascending and descending, will be validated separately.

For Validation Approach #1, we will use unwrapped interferograms at 100-m resolution to produce point-to-point relative LOS measurements (and their associated uncertainties) between GNSS sites. Position observations from the same set of GNSS sites and at the InSAR acquisition times will be projected into the LOS direction and differenced pairwise. These will be compared to the point-to-point InSAR LOS

measurements using a methodology similar to that described in Section 2.2.2., except that the accuracy specification is $3(1+L^{1/2})$ mm over 0.1 km < L < 50 km.

To validate the noise in individual interferograms using Validation Approach #2, we will utilize interferograms over the set of non-deforming sites discussed in Section 2.2.1. In practice, characterization of transient deformation will usually be improved by examining longer time series of interferograms. The approach described here validates the requirement that short timescale or temporally complex transients can be characterized with a single interferogram.

Validation Approach #3 uses measurements from UAVSAR across an area that is well characterized with GNSS stations. This could be an area of known deformation, such as a creeping section of the San Andreas Fault.

Comprehensive validation requires transient sites possessing different deformation characteristics (e.g., volcanoes, landslides, aquifers, hydrocarbons, etc.), vegetation covers (forest, shrub, bare surface, etc.), seasonality (leaf on/off, snow, etc.), and terrain slopes. The NISAR Science Team will select a set of cal/val regions to be used for this requirement and will list those sites in the NISAR cal/val plan.

2.3. Technical Framework for Validating Requirements

All of the analyses below will be performed independently on ascending and descending NISAR scenes to meet the terms of the L2 requirements.

2.3.1. Generalized Time Series Analysis

The InSAR and GNSS comparisons for Requirements 658 and 660 described in Section 2.2 will be performed using the framework of generalized time series analysis, whereby information in each time series is characterized by one or more underlying basis functions. The problem is cast as an overdetermined least squares (LSQ) estimation problem, from which we infer parameters for the simultaneous fit of various components to the time series, on a station-by-station or pixel-by-pixel basis. We describe our implementation of this approach in Section 4.

These components—which include secular velocities, seasonal sinusoids, temporal step offsets, and postseismic exponential decay—represent much of the non-stochastic variance in the time series and are well-suited to the specific validation targets. To perform the validations in Section 2.2, estimates of the fit parameters for these functions (rather than the raw time series themselves) will be used. For Requirement 658 (secular deformation) we will use the velocity component of these fits, while for Requirement 660 (coseismic deformation) we will use the velocity, Heaviside (instantaneous step), and (optionally) exponential/logarithmic postseismic components.

2.3.2. Spatial Analysis of InSAR scenes

In non-deforming regions, we conduct covariance analysis of LOS displacements within individual unwrapped interferograms (Requirement 663) or LOS

displacements/velocities in interferometric time series (Requirement 658 and 660). For this analysis, we calculate displacement/velocity residuals between randomly sampled points spanning baseline distances of 0.1~50 km within the analysis region (e.g., Lohman & Simons, 2005) (see Section 4.2). We compare the observed residual values to their associated threshold noise values at each baseline to validate that the observations pass mission requirements. We use ensemble statistics over different terrains and seasons for this validation approach. SES members have done relevant work in the past to validate the NISAR performance tool (Hensley et al., 2016) using the 70-km swath of ALOS interferograms, and before the NISAR launch, we will use ALOS-2 wide-swath or Sentinel-1 scenes to conduct this validation.

2.3.3. Comparison with UAVSAR

We make temporally coincident UAVSAR measurements of an area imaged by NISAR (Sentinel/ALOS-2 for now) to examine the spectrum of responses at distances shorter than GNSS station baselines. This provides information needed for the shorter component of the validation baseline. UAVSAR measurements should include a non-deforming region with corner reflectors such as the Rosamond Lakebed and deforming regions. Deforming regions should include those with rapid deformation in three components such as the Slumgullion landslide in Colorado and one component of motion such as the horizontally creeping central San Andreas fault or Hayward fault. Measurements should be made to optimize determination of absolute motions and in NISAR ascending and descending flight path directions for matching NISAR measurements. GNSS station motions should be used in the UAVSAR baseline adjustment. Individual interferograms can be used for rapidly deforming regions (e.g., Slumgullion landslide) and non-deforming regions (Rosamond), and time series spatial analysis for any areas with a stack of coincident measurements.

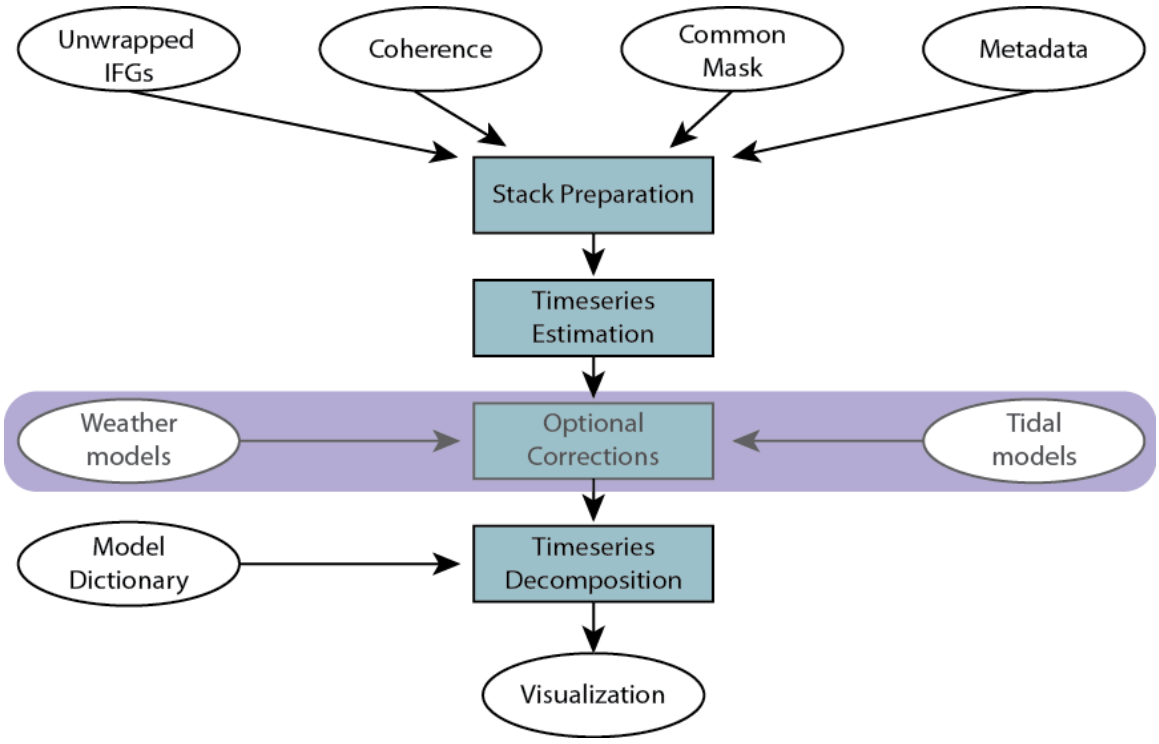

Figure 1: NISAR L3 product generation workflow for Requirements 658 (secular deformation rate) and Requirement 660 (co-seismic displacements).

3. L3 DATA PRODUCTS: GENERATION

3.1. Interferogram Stack Preparation

The project will provide sets of fully coregistered and geocoded ascending and descending unwrapped L2 interferograms (aka interferogram "stacks") over regions of interest listed in the NISAR Solid Earth Science cal/val document. As part of L2 processing, the project will calculate and apply standard (and possibly optional) corrections to minimize errors due to non-geophysical sources. An example of a standard correction for NISAR is the removal of ionospheric propagation delays using split-band processing.

InSAR stacks will include at a minimum nearest-neighbor and skip-1 interferograms, which represents the planned standard L2 data product from NISAR. A more complete set of interferograms, including pairs spanning longer periods, may be requested for regions with higher vegetation cover, soil moisture and/or snow cover variability. While the transient requirement can be validated using individual interferograms from these stacks, the time series used for the secular and coseismic requirements should be as long

as possible to improve fitting of seasonal basis functions and other time series components (note that the formal test of these requirements specifies a full three years of data).

For the purpose of testing ATBD algorithms prior to NISAR launch, the NISAR SES team will make interferogram stack using SAR data from complementary missions (e.g., Sentinel-1 or ALOS-2). For operational NISAR processing using ARIA geocoded unwrapped (GUNW) standard products, the following information will be provided in the Level-2 products provided for NISAR SES L2 requirements validation:

- Unwrapped ionosphere-corrected interferograms (either in radar or ground coordinates) following the L1 and L2 product descriptions summarized in the NISAR Handbook (2018). The spatial resolution of the interferograms must be 100 m or better (in order to address requirements 660 and 663).
- Corresponding coherence.
- Perpendicular baseline associated with the interferograms.
- Radar simulation containing pixel elevations.
- Radar incidence angles for each InSAR pixel.
- Shadow, layover and land/water masks corresponding to the interferograms.
- Configuration that includes processing parameters such as coherence thresholds, flags for applying phase corrections etc. to allow for region-specific customization.
- Solid Earth tide phase screen
- Optional: Atmospheric delay metadata
- Optional: Ocean tidal load response

3.2. Generation of time series from sets of interferograms

InSAR time series (i.e., the unfiltered displacement of each pixel vs. time) are estimated from a processed InSAR stack from Section 3.1 (either ascending or descending) using a variant of the small baseline subset (SBAS) approach and then parameterized using the approach described in Section 4. This step uses tools available in the MintPy software package (*Yunjun et al., 2019*), which provides both SBAS time series and model-based time series parameterization. As we expect high-quality orbital control for NISAR, we anticipate that the interferogram stack will typically include all nearest-neighbor (~12-day) and skip-1 (~24 day) interferograms, which will be the minimum inputs into the SBAS time series generation step. We note that recent results on InSAR closure phase and "fading signal" effects recommend the of use all available interferograms to avoid systematic bias (*Ansari et al.*, 2020; *Zheng Y.J. et al.,* 2022), and we will assess if additional interferograms are needed for validation.

3.2.1. Pre-Processing

We use the open-source ARIA-tools package to download processed Sentinel-1 GUNW interferograms over selected cal/val regions from the Alaska Satellite Facility

archive and to stitch/crop the frame-based NISAR-prototype GUNW products to stacks that can be directly ingested into MintPy for time-series processing. ARIA-tools uses a phase-minimization approach in the product overlap region to stitch the unwrapped and ionospheric phase (if available), a mosaicking approach for coherence and amplitude, and extracts the geometric information from the 3D data cubes through a mosaicking of the 3D datacubes and subsequent intersection with a DEM. We note that NISAR-prototype GUNW interferograms derived from Sentinel-1 using ARIA-tools have revealed interseismic deformation and creep along the San Andreas Fault system, along with subsidence, landsliding, and other signals.

We use MintPy to validate and modify the InSAR stack, removing interferograms that do not meet minimum coherence criteria, generating a quality control mask for the purpose of identifying noisy pixels within the stack, and referencing estimated deformation to a common location in all interferograms.

3.2.2. SBAS Line-of-Sight Timeseries Generation

InSAR time series generation will be performed using the MintPy software suite (*Yunjun et al., 2019*), which is open source and freely available. This toolbox has been used in many studies and will continue to be updated (with separate documentation) on a regular basis. MintPy is a suite of Python libraries and scripts that implement InSAR time-series processing algorithms in a common framework, including interferogram stack quality control, rapid generation of time-series products, and direct comparison of InSAR time-series with GNSS using different algorithms. The MintPy workflows we use to generate displacement timeseries are documented in code and text in separate Jupyter notebooks that accompany this document.

3.3. Optional Corrections

Phase distortions related to solid earth tides, ocean tide effects, and temporal variations in the vertical stratification of the atmosphere can be mitigated using the corrections described below. At this point, it is expected that these corrections will not be needed to validate the mission requirements, but they may be used to produce the highest quality data products. Typically, these are applied to the estimated time series product rather than to the individual interferograms, since they are a function of the time of each radar acquisition.

Optional tide corrections: Corrections for deformation due to the solid earth tide can be calculated using PySolid, which is built in the MintPy based on codes from *Milbert* (2018). Because the science requirements specify spatial scales of 50 km and shorter, the long-wavelength solid Earth tide is unlikely to be the source of significant errors. Corrections for ocean-tide loading can be calculated using the SPOTL toolbox (*Agnew*, 2012), which provides access to a collection of global and regional ocean models and allows for an easy combination of these models. Optimal configurations for ocean tide modeling will be studied in Phase C.

***Optional atmospheric correction**:* We optionally correct topography-correlated differential atmospheric delay in interferometric phase measurement following Doin et al. (2009) and Jolivet et al. (2011). These corrections are calculated from atmospheric data provided by Global Atmospheric Models (hereafter GAMs), such as ERA-Interim or its replacement ERA-5 (European Center for Medium-Range Weather Forecast Re-Analysis version 5), MERRA (Modern-Era Retrospective Analysis, Goddard Space Flight Center, NASA), or regional models such as NARR (North American Regional Reanalysis, National Oceanographic and Atmospheric Administration).

We utilize PyAPS (*Jolivet et al.*, 2011, *Jolivet and Agram*, 2012) to implement tropospheric phase delay corrections. PyAPS is well-documented and well-maintained and can be freely downloaded (http://pyaps.googlecode.com). PyAPS currently includes support for ECMWF's ERA-Interim, NOAA's NARR and NASA's MERRA weather models. A final selection of atmospheric models to be used for operational NISAR processing will be done during Phase C.

PyAPS determines the atmospheric phase delay on each pixel of each interferogram from the 3D distribution of atmospheric variables. For a given GAM dataset, we select grid points overlapping with the spatial coverage of the SAR scene. Atmospheric variables are provided at precise pressure levels. We vertically interpolate these values to a regular grid between the surface and a reference altitude, z_{ref}, above which the delay is assumed to be nearly unchanged with time (~30,000 m). Then the delay function on each of the selected grid points of the GAM is computed as a function of height. The LOS single path delay $\delta L^s_{LOS}(z)$ at an elevation z is given by (*Doin et al.,* 2009, *Jolivet et al.*, 2011):

$$\delta L^s_{LOS}(z) = \frac{10^{-6}}{cos(\theta)}\{\frac{k_1 R_d}{g_m}(P(z) - P(z_{ref})) + \int_z^{z_{ref}} \left(\left(k_2 - \frac{R_d}{R_v}k_1\right)\frac{e}{T} + k_3\frac{e}{T^2}\right)dz\} \qquad (1)$$

where θ is the local incidence angle, $R_d = 287.05\, J\, kg^{-1}\, K^{-1}$ and $R_v = 461.495\, J\, kg^{-1}\, K^{-1}$ are the dry air and water vapor specific gas constants, g_m is a weighted average of the gravity acceleration between z and z_{ref}, P is the dry air partial pressure in Pa, e is the water vapor partial pressure in Pa, and T is the temperature in K. The constants are $k_1 = 0.776\, K\, Pa^{-1}$, $k_2 = 0.716\, K\, Pa^{-1}$, and $k_3 = 3.75 \cdot 10^3 K^2 Pa^{-1}$.

The absolute atmospheric delay is computed at each SAR acquisition date. For a pixel at an elevation *z* at a specific acquisition date, the four surrounding grid points are selected and the delays for their respective elevations are computed. The resulting delay at the pixel of interest is then the bilinear interpolation between the delays at the four grid points. Finally, we combine the absolute delay maps of the InSAR partner images to produce the differential delay maps used to correct the interferograms. Details and validation of the PyAPS approach are available in *Doin et al.* (2009) and *Jolivet et al.* (2012).

4. L3 DATA PRODUCTS: VALIDATION

The approach used for the generation of NISAR L3 products for Requirements 658 (secular deformation rate) and Requirement 660 (co-seismic displacements) allows for the explicit inclusion of key basis functions (e.g., Heaviside functions, secular rate, etc.) in the InSAR inversion. Modifications to this algorithm may be identified and implemented in response to NISAR Phase C activities.

4.1. Decomposition of InSAR and GNSS time series into basis functions

Given a time series of InSAR line-of-sight (LOS) displacements, the observations for a given pixel, $U(t)$, can be parameterized as:

$$U(t) = a + vt + c_1 cos\,(\omega_1 t - \phi_{1,}) + c_2 cos\,(\omega_2 t - \phi_2) + \sum_{j=1}^{N_{eq}} \left(h_j + f_j F_j(t - t_j)\right) H(t - t_j) + \frac{B_\perp(t)}{R sin\theta} \Delta z + residual$$

(2)

which includes coefficients for constant offset (a), velocity (v), and amplitudes (c_j) and phases (ϕ_j) of annual (ω_1) and semiannual (ω_2) sinusoidal terms. Where needed, we include additional complexity, such as coseismic and postseismic processes parameterized by Heaviside (step) functions *H* and postseismic functions *F* (typically exponential and/or logarithmic), with coefficients are *h* and *f*. $B_\perp(t)$, R, θ, and Δz are, respectively, the perpendicular component of the interferometric baseline relative to the antenna position on the first date of the time series, slant range distance, incidence angle, and topographic estimation error (e.g., *Fattahi and Amelung*, 2013) for the given pixel.

This parameterization of ground deformation has a long heritage in geodesy, originally in the analysis of GNSS time series and now with InSAR data (e.g., *Blewitt,* 2007, *Hetland et al*., 2012, *Agram et al*., 2013). We perform the same parameterization on GNSS time series within the footprint of the InSAR stack., using MintPy to find and download GNSS displacement time series from the Nevada Geodetic Laboratory (University of Nevada, Reno) archive. We use MintPy to project the three GNSS displacement components into the radar line of sight using the LOS vectors provided in the L2 data product for each pixel.

Given an ensemble of interferograms or the output of an SBAS (displacement vs. time) estimator, we can write the least squares (LSQ) basis function fitting problem as

$$\mathbf{Gm} = \mathbf{d} \qquad (3)$$

where **G** is the design matrix (constructed from the different functional terms in Equation 2, evaluated at the SAR image dates for SBAS output or between the dates spanned by each pair for interferograms), **m** is the vector of model parameters (with coefficients given in Equation 2) and **d** is the vector of observations. For GNSS time series, **G, d,** and

m, are constructed using values evaluated at daily epochs corresponding to valid GNSS solutions. For SBAS InSAR input, these epochs are typically the SAR acquisition dates for all the InSAR pairs. Equation 3 can be solved as a conventional weighted LSQ solution for the maximum likelihood model, where we minimize the L2 norm of the weighted misfit (e.g., *Aster et al*., 2013):

$$argmin\ \varphi(\mathbf{m}) = (\mathbf{d} - \mathbf{Gm})^T \mathbf{C_d}^{-1} (\mathbf{d} - \mathbf{Gm}) \quad (4)$$

Here, the data covariance matrix $\mathbf{C_d}$ is constructed using the empirical estimate of correlation from each contributing interferogram over the appropriate subset of pixels (i.e., masking out water bodies and regions that are decorrelated, such as agricultural fields) and superscript T denotes matrix transpose. Only pixels that are coherent in most interferograms are used as input to the construction of $\mathbf{C_d}$. The solution for this overdetermined minimization problem can be written as

$$\mathbf{m_{est}} = \mathbf{G^{-g}d} \quad (5)$$

where

$$\mathbf{G^{-g}} = [\mathbf{G}^T \mathbf{C_d}^{-1} \mathbf{G}]^{-1}\ \mathbf{G}^T \mathbf{C_d}^{-1} \quad (6)$$

The full covariance on the estimated parameters, $\mathbf{C_m}$, can be estimated from

$$\mathbf{C_m} = \mathbf{G^{-g}} \mathbf{C_d} \mathbf{G^{-gT}} \ . \quad (7)$$

With this formulation, we can obtain GNSS and InSAR velocity estimates and their formal uncertainties (including in areas where the expected answer is zero).

4.2. NISAR Validation Procedure

We use three complementary approaches to validate the L2 Requirements. These validation approaches are needed to understand the limits of performance as completely as possible given existing limitations on resources and the distribution of cGNSS networks.

4.2.1. cGNSS-InSAR direct comparison (Validation Approach #1)

Here we compare either the individual unwrapped interferograms or the parameterized time series (linear + seasonal + offsets + exponential components) from the InSAR stack with GNSS, across the length scales defined in the L2 requirements. We first calculate the difference of the relevant time series parameter (secular deformation rate for Requirement 658, or co-seismic displacement for Requirement 660) or the interferogram displacement (for Requirement 663) between all possible pairs of cGNSS locations within a validation region. This gives the vectors $\Delta\mathbf{m}_{\mathbf{est,cGNSS}}$ and $\Delta\mathbf{m}_{\mathbf{est,InSAR}}$, along with the baseline distance L between locations. We then calculate the residual differences between vectors $\Delta\mathbf{m}_{\mathbf{est,cGNSS}}$ and $\Delta\mathbf{m}_{\mathbf{est,InSAR}}$, bin them by baseline distance L, and obtain the percentage of the residuals in each bin whose absolute value lies below the thresholds defined in each of the SES L2 requirements. (Note: the threshold is a single

value for the secular rate requirement, and a baseline-dependent curve for the coseismic and transient requirements).

We assume that the residuals between GNSS and InSAR follow a Gaussian distribution. For each 5 km-wide distance bin, if the fraction of residuals lying below the bin threshold value is more than 0.683 (i.e., one standard deviation), we judge displacements/velocity to pass the requirement test. For the mission to meet the solid earth requirements more broadly, only 70% of all interferograms in high-deformation regions (secular), in regions experiencing significant earthquakes (coseismic), or over selected transient targets (transient) have to pass the requirement test for all bins.

4.2.2. InSAR noise analysis (Validation Approach #2)

For Validation Approach #2, we evaluate estimated deformations/velocities over selected cal/val areas with negligible deformation. Any non-zero deformation/velocity should thus be treated as noise, and our goal is to evaluate the statistical significance of this noise. Actual noise in InSAR displacements/velocities is likely to be anisotropic, but here we neglect this anisotropy. Also, we assume the noise is stationary.

We first randomly select pixels from within the analysis region and pair up the pixel samples. For each pixel-pair, the difference of their measurement is:

$$d(r) = |(f(x) - f(x - r))| \quad (8)$$

Estimates of $d(r)$ from all pairs are binned according to the distance r. In each bin, $d(r)$ is assumed to be a normal distribution.

Our method to evaluate the noise structure is similar to that in Section 4.2.1, except that the percentage of measurements that fall below the threshold curve is first calculated for each of the 5-km-wide bins, then averaged across all bins. If the average from all bins is larger than 0.683, we judge that the noise level falls below the requirement.

4.2.3. UAVSAR Comparison (Validation Approach #3)

Direct UAVSAR-NISAR comparisons over selected deforming and non-deforming areas will follow the same formalism as specified in 4.1 but with the addition of the UAVSAR InSAR displacement vs. time to the GNSS validation data. From this, the procedures given in 4.2.1 apply, again with the comparison now including both GNSS and UAVSAR InSAR to produce residual differences. Point-to-point measurements required to validate the coseismic requirement in a deforming region can be obtained in creeping section of the San Andreas fault where there is also reasonable GNSS coverage.

UAVSAR can also be used to quantify deformation variation across a nominally "zero" deforming swath and to characterize other NISAR error sources, such as uncorrected ionosphere and troposphere path delay variations. UAVSAR measurements will be collected in selected SES cal/val areas where there is good GNSS coverage to quantify possible surface motion and confirm zero deformation outside of the point GNSS locations. Variation in UAVSAR throughout the target regions of interest should be quantified in order to anticipate expected variation in NISAR products

5. ASSUMPTIONS AND REQUIRED INPUT

The cal/val activities covered by this ATBD assume:

- The project will provide sets of fully coregistered ascending and descending unwrapped L2 interferograms (aka InSAR "stacks") over regions of interest listed in the NISAR Solid Earth cal/val document. For the purpose of testing cal/val algorithms prior to NISAR launch, the NISAR SE team will make interferogram stack using SAR data from complementary missions (e.g., Sentinel-1 or ALOS-2). These stacks will include at a minimum nearest-neighbor and skip-1 interferograms to mimic the planned standard L2 data product from NISAR, and they will span a minimum of 2 years to support full testing of the validation algorithms for all three L2 requirements (including the fitting of seasonal basis functions to the InSAR time series). A more complete set of interferograms, including pairs spanning longer periods, may be requested for regions with higher vegetation cover, soil moisture and/or snow cover variability. The format of these interferograms will be consistent with the GIANT analysis package (*Agram et al*., 2013), which will be used to generate L3 time series data products.

- As part of L2 processing, the project will calculate and apply standard corrections to minimize errors due to non-geophysical sources. An example of a standard correction is the removal of ionospheric propagation delays using split-band processing (e.g., *Rosen et al*., 2010; *Gomba et al.,* 2016; *Liang and Fielding*, 2017; *Fattahi et al*., 2017).

- The project will have access to L2 position data for GNSS stations in third-party networks such NSF's Plate Boundary Observatory, the HVO network for Hawaii, GEONET-Japan, and GEONET-New Zealand, located in target regions for NISAR solid earth cal/val. Station data will be post-processed by one or more analysis centers, will be freely available, and will have latencies of several days to weeks, as is the case with positions currently produced by the NSF's GAGE Facility and separately by the University of Nevada Reno. Networks will contain one or more areas of high-density station coverage (2~20 km nominal station spacing over 100 x 100 km or more) to support validation of L2 NISAR requirements at a wide range of length scales.

6. PLANNED DELIVERABLES

L3 products to be produced by the NISAR Solid Earth Science team will include:

- Maps of locations where the InSAR and GNSS data are being compared.
- In the case of secular and coseismic requirements:
    - The InSAR line-of-sight displacement time series at each GNSS station location, and the corresponding (LSQ-estimated) functional fit to the displacements.

    - The GNSS line-of-sight displacement time series at each GNSS station location, and the corresponding (LSQ-estimated) functional fit to the displacements.
    - A specification of the approach used to generate the InSAR time series from the underlying interferograms.
- Tables and/or figures of comparisons showing GNSS/InSAR (Approach #1) and InSAR-only (Approach #2) residuals of velocities, co-seismic displacements, and transient displacements as a function of baseline distance.

7. REFERENCES

NISAR, 2018. NASA-ISRO SAR (NISAR) Mission Science, Users' Handbook. NASA Jet Propulsion Laboratory. 261 pp, https://nisar.jpl.nasa.gov/system/documents/files/26_NISAR_FINAL_9-6-19.pdf

Agnew, D.C., SPOTL: Some Programs for Ocean-Tide Loading, SIO Technical Report, Scripps Institution of Oceanography, http://escholarship.org/uc/item/954322pg, 2012.

Agram, P.S., R. Jolivet, B. Riel, Y.N. Lin, M. Simons et al., New Radar Interferometric Time Series Analysis Toolbox Released, EOS Transactions, 94, 7, 69-70, 2013.

Aster, R.C., B. Borchers, and C.H. Thurber, Parameter Estimation and Inverse Problems, 2nd edition, Elsevier Academic Press, 2013.

Bamler, R. and P. Hartl, Synthetic aperture radar interferometry, Inverse Problems, 14, R1—R54, 1998.

Berardino, P., G. Fornaro, R. Lanari, and E. Sansosti, A new algorithm for surface deformation monitoring based on small baseline differential SAR interferograms, IEEE Trans. on Geosci. and Rem. Sens., 40, 2375–238, 2002.

Blewitt, G., GPS and space based geodetic methods, in Treatise on Geophysics, vol. 3, edited by T. Herring, pp. 351– 390, Academic, Oxford, U.K., 2007.

Bürgmann, R., P.A Rosen, and E.J. Fielding, Synthetic aperture radar interferometry to measure Earth's surface topography and its deformation, Annual Review of Earth and Planetary Sciences, 28(1), pp.169-209, 2000.

Doin, M-P., C. Lasserre, G. Peltzer, O. Cavalié, and C. Doubre, Corrections of stratified tropospheric delays in SAR interferometry: Validation with global atmospheric models, Journal of Applied Geophysics, 69(1), pp. 35-50, 2009.

Doin, M.P., S. Guillaso, R. Jolivet, C. Lasserre, F. Lodge, G. Ducret, and R. Gradin, Presentation of the small baseline NSBAS processing chain on a case example: The Etna deformation monitoring from 2003 to 2010 using Envisat data. In FRINGE 2011 ESA Conference, Frascati, Italy, September 2011. ESA.

Donnellan, A., J. Green, A. Ansar, R. Muellerschoen, J. Parker, A. Tanner, Y. Lou, M. Heflin, R. Arrowsmith, J. Rundle, Y. Ben-Zion, S. DeLong, L. Grant Ludwig, 2018, July. Geodetic Imaging of Fault Systems from Airborne Platforms: UAVSAR and Structure from Motion. In IGARSS 2018-2018 IEEE International Geoscience and Remote Sensing Symposium (pp. 7878-7881). IEEE.

Duputel, Z., J. Jiang, R. Jolivet, M. Simons et al., The Iquique earthquake sequence of April 2014: Bayesian modeling accounting for prediction uncertainty, Geophys. Res. Lett., doi:10.1002/2015GL065402, 2015.

Fattahi, H., and F. Amelung, DEM error correction in InSAR time series. IEEE Transactions on Geoscience and Remote Sensing, 51(7), 4249-4259, 2013.

Fattahi, H., Simons, M. & Agram, P., 2017. InSAR Time-Series Estimation of the Ionospheric Phase Delay: An Extension of the Split Range-Spectrum Technique, IEEE Transactions on Geoscience and Remote Sensing, 55, 5984-5996.

Goldstein, R. M., H. Engelhardt, B. Kamb and R. M. Frolich, Satellite Radar Interferometry for Monitoring Ice Sheet Motion: Application to an Antarctic Ice Stream, Science, 262, 1525-1530, 1993.

Gomba, G., A. Parizzi, F. De Zan, M. Eineder and R. Bamler, Toward Operational Compensation of Ionospheric Effects in SAR Interferograms: The Split-Spectrum Method, IEEE Trans. Geosci. Rem. Sens., 54, doi:10.1109/TGRS.2015.2481079, 1446-1461, 2016.

Hanssen, R. A., Radar Interferometry: Data Interpretation and Error Analysis, Springer, New York, 2001.

Hensley, S.H., P. Agram, S. Buckley, H. Ghaemi, E. Gurrola, L. Harcke, C. Veeramachaneni and S-H Yun, NISAR Performance Modeling and Error Budget, Jet Propulsion Laboratory, Interoffice Memorandum, January 26, 2016.

Hetland, E. A., P. Musé, M. Simons, Y. N. Lin, P. S. Agram, and C. J. DiCaprio, Multiscale InSAR time series (MInTS) analysis of surface deformation, Journal of Geophysical Research: Solid Earth, 117(B2), 2012.

Hooper, A., Persistent Scatterer Radar Interferometry for Crustal Deformation Studies and Modeling of Volcanic Deformation, PhD Thesis, Stanford University, 2006.

Jolivet, R., R. Grandin, C. Lasserre, M.- P. Doin, and G. Peltzer, Systematic InSAR tropospheric phase delay corrections from global meteorological reanalysis data, Geophysical Research Letters, 38(17), 2011.

Jolivet, R. and P. S. Agram, Python-based atmospheric phase screen mitigation using atmospheric re-analysis, 2012. URL: http://pyaps.googlecode.com.

Jolivet, R., C. Lasserre, M.-P. Doin, S. Guillaso, G. Peltzer, R. Dailu, J. Sun, Z.-K. Shen, and X. Xu, Shallow creep on the Haiyuan fault (Gansu, China) revealed by SAR interferometry, Journal of Geophysical Research: Solid Earth, 117(B6), 2012.

Jolivet, R., P. Agram, Y.N. Lin, M. Simons, M.-P. Doin, G. Peltzer, and Z. Li, Improving InSAR geodesy using Global Atmospheric Models, J. Geophys. Res., doi 10.1002/2013580/10558, 2014.

Liang, C., and E. J. Fielding, Interferometry with ALOS-2 full-aperture ScanSAR data. IEEE Transactions on Geoscience and Remote Sensing, 55(5), 2739-2750, 2017.

Lohman, R, and M. Simons, Some thoughts on the use of InSAR data to constrain models of surface deformation: Noise structure and data downscaling, Geochemistry, Geophysics, Geosystems, 6(1), doi:10.1029/2004GC000841, 2005.

Lyons, S., and D. Sandwell. Fault creep along the southern San Andreas from interferometric synthetic aperture radar, permanent scatterers, and stacking. Journal of Geophysical Research: Solid Earth 108.B1, doi:10.1029/2002JB001831, 2003.

Massonnet D., M. Rossi, C. Carmona, F. Adragna, G. Peltzer, K. Feigl and T. Rabaute, The displacement field of the Landers earthquake mapped by radar interferometry, Nature, 364, 138-142, doi:10.1038/364138a0, 1993.

Massonnet, D. and K. L. Feigl, Radar interferometry and its application to changes in the earth's surface, Review of Geophysics, 36, 441-500, 1998.

Milbert, D., "solid: Solid Earth Tide", [Online]. Available: http://geodesyworld.github.io/SOFTS/solid.htm, 2018.

Pritchard, M. E., C. Ji, and M. Simons, Distribution of slip from 11 Mw > 6 earthquakes in the northern Chile subduction zone, J. Geophys. Res., 111, doi: 10.1029/2005JB004013, 2006.

Pritchard, M. E., E. O. Norobuena, C. Ji, R. Boroscheck, D. Comte, M. Simons, T. H. Dixon, and P. A. Rosen, Geodetic, teleseismic, and strong motion constraints on slip from recent southern Peru subduction zone earthquakes, J. Geophys. Res., 112, B03307, doi:10.1029/2006JB004294, 2007.

Rosen, P.A., S. Hensley, I.R. Joughin, F.K. Li, S.N. Madsen, E. Rodriguez and R.M. Goldstein, Synthetic aperture radar interferometry, Proceedings of the IEEE, 88(3), pp.333-382, 2000.

Rosen, P. A., S. Hensley, and C. Chen, Measurement and mitigation of the ionosphere in L-band interferometric SAR data, In Radar Conference, IEEE, 1459-1463, 2010.

Rosen, P. A., E. Gurrola, G. F. Sacco, and H. Zebker, The InSAR scientific computing environment, In Synthetic Aperture Radar, 2012. EUSAR. 9th European Conference on, pp. 730-733. VDE, 2012.

Simons, M. and P.A. Rosen, Treatise on Geophysics, Interferometric Synthetic Aperture Radar Geodesy, Schubert, G. (ed.), M. Simons et al., 2nd Ed., Volume 3- Geodesy, Elsevier Press, 339-385, 2015.

Snedecor, G.W. and W.G. Cochran, Statistical Methods, Eighth Edition, Iowa State University Press, 1989.

Williams, S., Y. Bock, and P. Fang, Integrated satellite interferometry: Tropospheric noise, GPS estimates, and implication for interferometric synthetic aperture radar products, J. Geophys. Res., 103, 27,051 – 27,067, 1998.

Yunjun, Z., H. Fattahi, and F. Amelung, Small baseline InSAR time series analysis: Unwrapping error correction and noise reduction, Computers & Geosciences, 133, 104331, doi:10.1016/j.cageo.2019.104331, 2019.

Zebker, H. P. A. Rosen, R. M. Goldstein, A. Gabriel and C. L. Werner, On the derivations of coseismic displacement fields using differential radar interferometry: The Landers earthquake, J. 99, 19617-19634, 1994.